Carbon 96 (2016) 83–90

Contents lists available at ScienceDirect

Carbon

journal homepage: www.elsevier.com/locate/carbon

Multilayer stacking and metal deposition effects on large area graphene on GaAs

Hong-Yeol Kim [a, *], Omar M. Dawood [a, b], Umberto Monteverde [a], James Sexton [a], Zheling Li [b], Liam Britnell [c], Max A. Migliorato [a], Robert J. Young [b], Mohamed Missous [a]

[a] School of Electrical and Electronic Engineering, University of Manchester, Sackville Street, Manchester M13 9PL, UK
[b] School of Materials, University of Manchester, Oxford Road, Manchester M13 9PL, UK
[c] BGT Materials Ltd, Photon Science Institute, University of Manchester, Oxford Road, Manchester, M13 9PL, UK

ARTICLE INFO

Article history:
Received 31 March 2015
Received in revised form
29 July 2015
Accepted 4 September 2015
Available online 9 September 2015

Keywords:
Large area
Multilayer
CVD graphene
Raman spectroscopy
Sheet resistance

ABSTRACT

Graphene was grown on copper and repeatedly transferred onto a GaAs semi-insulating substrate to form multilayers (1–10). These manually stacked graphene layers resulted in appreciable local variations of optical properties due to the local differences of stacking orders. In addition, most of the observed 2D/G intensity and area ratios of an n-multilayer CVD graphene is consistent with the characteristics of a single layer repeated n-times. However, multilayer graphene has many kinds of advantages for applications to optoelectronic devices. First, the G band shift is not related to the stacking order, proving that multilayer graphene reduces doping and strain effect from the substrate, which is confirmed by Raman results after metal electrode deposition. Second, the sheet resistance decreases with increasing number of layers and after thermal annealing. Another benefit of multilayer graphene is that each layer can be annealed after transfer, which greatly improves the sheet resistance and its lateral uniformity without intentional doping. We therefore conclude that multilayer CVD graphene is a good candidate for various GaAs-based electrical applications and its good electrical uniformity allows fabrication of devices on large scales.

1. Introduction

From its isolation in 2005 [1], graphene has been extensively investigated and many papers have been published reporting outstanding carrier mobility, transparency, thermal conductivity and physical strength. However, most of these properties were observed under limited conditions such as micro sized exfoliated graphene flakes from Highly Ordered Pyrolytic Graphite (HOPG) [2,3] or highly doped graphene [4,5]. As for high volume manufacturing HOPG is not an ideal material whilst the limited information on large area graphene has somewhat impeded the development of electrical applications.

Chemical Vapor Deposited (CVD) graphene represents one of the solutions for large sized applications and mass production. It also allows control of the thickness of graphene by repeated transfer to achieve large numbers of stacked layers. Epitaxial growth of graphene on SiC by thermal decomposition is another method to obtain large area graphene, but it requires highly expensive SiC substrates and high processing temperature (1500–2000 °C) [6–8]. Contrary to the latter method, large sized monolayer graphene can be grown on less expensive substrates, such as copper, by CVD. There are, however, practical constraints on using monolayer CVD graphene mainly due to the introduction of various types of defects that degrade the properties. Since graphene is generally grown on polycrystalline copper, the differences in the crystallography of copper (mostly polycrystalline) affects the growth rate, which is the main cause of a large number of grain boundaries and point defects [9,10]. Although graphene has been well known for its mechanical strength, CVD graphene as a one-atom thick material is very fragile. This makes the transfer process on substrate a crucial step which is also the source of folds and tears on graphene. Therefore, large area graphene presents many defects resulting in low optical and electrical uniformity.

Multilayer CVD graphene has been experimented in different electrical contexts such as transparent electrodes [11,12], and transistors [13]. But in order to successfully introduce graphene in semiconductor device fabrication, one very important issue that

* Corresponding author.
E-mail address: hongyeol.kim@manchester.ac.uk (H.-Y. Kim).

http://dx.doi.org/10.1016/j.carbon.2015.09.014
0008-6223/

needs to be considered is that of yield in large area graphene. In this respect, graphene needs to be uniform [14] and the fabrication process must be nonintrusive.

In this work, to confirm the compatibility of multilayer graphene for electrical applications, large area CVD graphene layers were transferred on GaAs and their optical and electrical properties were investigated. In certain cases we have compared GaAs with SiO_2 substrates. SiO_2 has been widely used to characterize graphene and, hence, used as a metric of comparison also here. We have investigated the advantages and disadvantages of large area graphene transfer, along with the multi-staking as a way of improving the uniformity and carrier mobility. Consequences of the fabrication process were also considered, in particular the strain induced on graphene, supported by the semi-insulating GaAs, after metal deposition. GaAs is a well-known semiconductor for optoelectronics, ultrafast electronics and quantum electronics applications due to its direct bandgap and high electron mobility. Hybrid structure of graphene and GaAs can expand graphene applications as well as ultra-thin III–V nano-device applications.

2. Graphene: growth and transfer

Large area monolayer graphene on Cu was synthesized by BGT materials Ltd using a large area CVD process. Monolayer graphene was grown on copper foils using the well-known hot wall CVD technique. Prior to growth, the copper foil was inserted into a quartz chamber and annealed for 30 min to help remove surface contaminants. Graphene was then grown on a copper foil at 1030 °C by allowing methane flow into the chamber for 30 min. The sample was then quickly cooled to room temperature, removed from the furnace and prepared for transfer on GaAs and SiO_2. Graphene was then spin coated with a solution of PMMA powder and chlorobenzene. Coated graphene on Cu was cured on a hot plate at 120 °C for 5 min. Low-quality graphene on the backside of Cu was removed by Reactive-Ion Etching (RIE) where the power of the plasma was 100 W and etching time was 3 min using a 50 SCCM oxygen flow rate. To dissolve the Cu substrate, 0.5 mol of an ammonium persulfate solution was used, where graphene/Cu remained floating on the surface of the solution for 1 h before the transfer to DI water. Semi-insulating GaAs substrates (1.5×1.5 cm^2 sized) were cleaned with acetone and isopropyl alcohol (IPA) then dipped in an HCl:H_2O (1:1) solution for 30 s to remove the native oxide, prior to graphene transfer. After transfer, graphene was dried at 70 °C on a hot plate and, subsequently, PMMA coating was removed in acetone for 90 min. Any n-multilayer graphene was obtained by reiterating the above procedure n-times.

3. Surface morphology: defects and contaminations

We investigated the suitability of using multilayer graphene for large scale manufacturing of electronic devices by investigating its spatial uniformity in optical measurements. Since graphene layers, especially on GaAs, are invisible with an optical microscope, it is difficult to estimate the number of layers or the generated defects by direct optical imaging. To investigate the surface morphology of the multilayer graphene layer, a bilayer film i.e. the simplest structure of multilayer graphene, was initially observed using SEM. As shown in Fig. 1, many kinds of defects were present including folded and scrolled graphene, tears and contamination with unknown particles as well as easily identifiable PMMA residue from the transfer process. Some of these originated during growth itself and others were generated during the transfer process. The folded graphene, often referred to as “wrinkle”, is due to the difference of thermal expansion coefficient between graphene and the copper substrate [15]. The tears can be generated by air pockets during the transfer process and removal of PMMA, as well as by the weak adhesion between graphene and substrate especially near the grain boundaries [16]. In addition, many graphene hexagonal domains are also created during growth, which generally extend for few layers [17,18]. It can be easily expected that most of these defects will affect the optical and electrical properties.

4. Raman spectroscopy for large area uniformity

A more accurate investigation of the graphene's conditions was carried out using Raman spectroscopy, which gives an account of defects, damages and doping [19–21].

For the micro-Raman characterization, a 514 nm wavelength laser was utilized at a power of 0.277 mW with a spot size on the graphene surface of 0.83 μm, when a 50× objective lens was used. A total of 16 points were measured in each sample arranged such that vertical and horizontal distances between points were 2 mm. Fig. S1(a) in the Supporting material shows the order and locations of the micro-Raman measurement points.

Raman measurements were performed on different samples having from 1 to 5 layers graphene to compare intensities and areas of G and 2D peaks. Prior to investigating the effects of different graphene layers on GaAs, Raman results of monolayer graphene on SiO_2/Si and GaAs were compared and shown in Table 1 where each value is an average of 12 and 16 (respectively) roughly equally spaced points measured on graphene/SiO_2 and graphene/GaAs. The 514 nm wavelength (2.4 eV) laser exceeds the bandgap of GaAs (1.42 eV) thus creating electron–hole pairs which, then, recombine producing luminescence that interferes with the detection of graphene vibrations. Therefore, to have more clean Raman results, the detection time for Raman scattering of graphene on GaAs should be 10 times longer than that of graphene on SiO_2/Si substrate where the presence of an indirect bandgap reduces this interference. The shift of the G and 2D bands, along with the intensity ratio of 2D and G (I_{2D}/I_G) were not very different, as visible from Table 1.

Further analysis of the characteristic graphene Raman peaks were carried out. In particular, the intensity ratio (I_{2D}/I_G) and the area ratio (A_{2D}/A_G) of 2D and G, for the five sample of GaAs with 1–5 layers of graphene, were compared. The intensities of G and 2D Raman modes were normalized to the Longitudinal Optic (LO) mode of GaAs (corresponding to a shift of 290 cm^{-1}). All normalized Raman peaks are shown in Fig. S1(b)–(f) in the Supporting material. Fig. 2 (a) and (b) show the box charts of I_{2D}/I_G and A_{2D}/A_G, respectively. The bars and the diamonds in Fig. 2(a) and (b) represent median and average value of the 16 measured points, respectively. In the same figure, the stars on the error bars indicate the minimum and the maximum value but those separated from the bars indicate the outliers which are very much bigger or smaller than other data points. The I_{2D}/I_G and A_{2D}/A_G are commonly used to identify the number of graphene layers exfoliated from graphite, as such ratios appear to be quantitatively and uniquely linked to the nature of the stacking between layers [18,22,23]. In our samples we conclude that the 2D/G ratios cannot be used to confirm the number of layers in the case of CVD graphene because of the large variations even for a nominally uniform sample area, as shown in Fig. 2(a) and (b). Such variations go well beyond what one would expect simply from imperfections in the layers. Except for the results of monolayer graphene, the other results show large ranges of the 2D/G ratios. The most reasonable explanation comes from the nature of the stacking of transferred graphene multilayers which is not the typical AB Bernal stacking generally seen in few layer graphene exfoliated from HOPG, which shows a decrease of the 2D/G ratios with increasing number of layers. Instead, the 2D/G ratio of turbostratic graphene looks similar to that of a monolayer graphene, as if the layers can be considered as independent from each

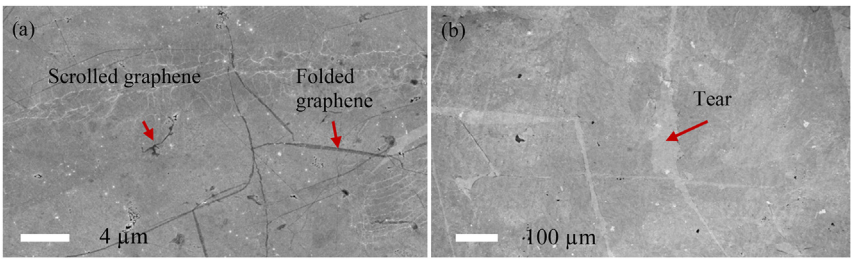

Fig. 1. SEM images of bilayer graphene where folded (wrinkle) and scrolled graphene as well as many particles were seen. (A colour version of this figure can be viewed online.)

Table 1
Comparison of Raman results and standard deviations (σ) of monolayer graphene on SiO_2/Si and semi-insulating GaAs substrates. Each value in results on SiO_2/Si and on GaAs is an average of 12 points and 16 points, respectively. The spacing between each measured point was 2 mm.

Monolayer graphene on SiO_2/Si (12P AVG)			Monolayer graphene on GaAs (16P AVG)		
G Pos.(cm^{-1}) (σ)	2D Pos.(cm^{-1}) (σ)	I_{2D}/I_G (σ)	G Pos.(cm^{-1}) (σ)	2D Pos.(cm^{-1}) (σ)	I_{2D}/I_G (σ)
1589.32 (2.53)	2691.73 (1.75)	2.36 (0.50)	1590.08 (2.17)	2690.65 (1.50)	2.36 (0.47)

other and each behaving as a collection of monolayer graphene [18]. The distributions of I_{2D}/I_G in each graphene layer shown in Fig. 2(c) supports this explanation. Almost 84% of the total I_{2D}/I_G ratios measured on the 2 to 5 layer graphene are over 1.5, which is comparable with the 94% of the I_{2D}/I_G ratio greater than 1.5 for the monolayer sample (see Fig. 2(c)). In addition, incomplete stacking due to interlayer particles and defects can also contribute to the measurements, as visible from the data variations in Fig. 2. Fig. 3(a) shows a schematic diagram of multilayer graphene on GaAs, where different colored areas in each layer graphene indicate the different directional graphene grains. Fig. 3 (b) and (c) show the AB Bernal stacking and mixed stacking structure, respectively. Although it is impossible to separate complete turbostratic, incomplete and Bernal stacking orders from each Raman-measured point, because some values of I_{2D}/I_G might result from a mix of the three stacking order, it is clear that the turbostratic and incomplete orders are not dominant but yet very significant.

Theoretical and experimental studies of epitaxial grown multilayer graphene on SiC showed similar results and proved that decoupling of twisted graphene layers make their band structure identical to isolated graphene [24,25]. These studies indicate that randomly stacked multilayers can behave like a single layer of graphene. Change in the intensities, areas, line widths and positions of each Raman features of multilayer CVD graphene on GaAs,

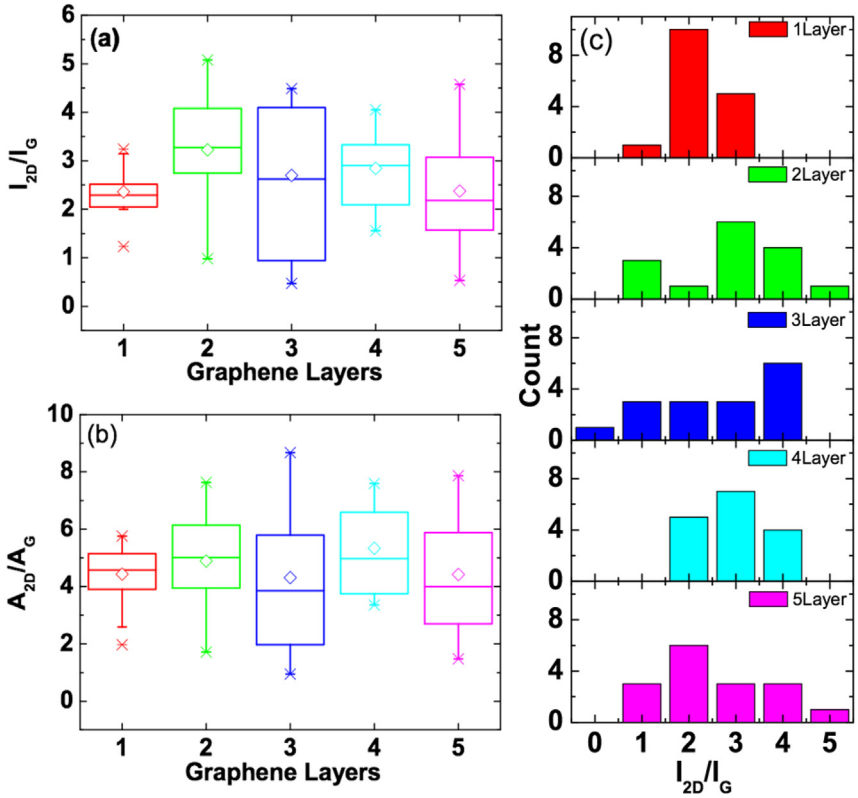

Fig. 2. Statistical Raman data: (a) Intensity ratio I_{2D}/I_G, (b) Area ratio A_{2D}/A_G of 2D and G, and (c) I_{2D}/I_G distributions for each sample (1–5 graphene layer on GaAs). (A colour version of this figure can be viewed online.)

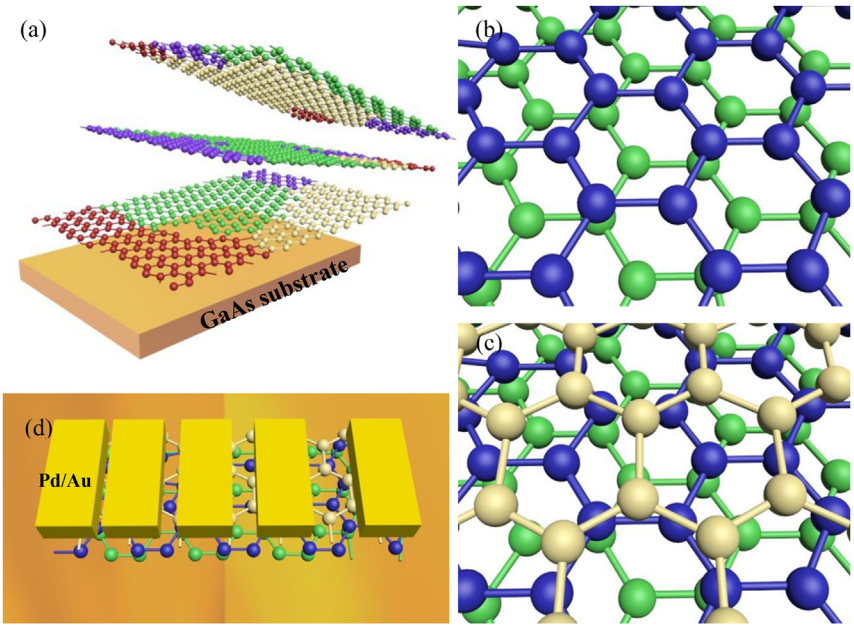

Fig. 3. Schematic diagram of transferred multilayer graphene: (a) graphene with different directional grain (indicated by different colors), grain boundaries and defects, (b) prospective view of a bilayer graphene with AB-Bernal stacking, (c) prospective view of three-layer graphene with mixed (Bernal and turbostratic) stacking structure, (d) TLM pattern on mixed-stacking graphene. (A colour version of this figure can be viewed online.)

shown in Fig. 4 (a)–(f), are consistent with earlier reports [24,25]. Different increase in the intensity and area of the G and 2D band with different stacked graphene structures were also reported in Ref. [18]. The G band areas of turbostratic and Bernal structures increase with the number of layers, but the rates of such increase are different in both stacking structures. Jih-Shang et al. [18] showed that the difference between the increase-rate slope of turbostratic and Bernal structures was larger over the 3 layers. The increasing trend of the G band areas with the number of layers are similar to the results of Jih-Shang et al. as shown in Fig. 4 (a). However, the variations of the G band area are gradually larger. This can be explained by the presence, locally, of a mixture of three different stacking orders which affect the G band area. This results in a larger variations with increase in the number of layers. On the other hand, since double resonance Raman scattering is sensitive to the band structure of multilayer structures [24,26], intensity and area of the 2D band are effected by different stacking orders. In contrast to the wider line shapes and smaller peak intensities of 2D band in Bernal stacking graphene [26,27], turbostratic graphene shows a similar line width to that of single layer but with larger intensity [18,28]. Superposition of 2D band in mixed stacking structure of multilayer graphene have larger line width and higher intensity than the 2D band of monolayer graphene.

The position of the G band decreases with the increase in the number of layers regardless of their stacking structures as shown clearly in Fig. 4(e). Such trend is entirely consistent with previous available reports that include the results of CVD, mechanically exfoliated graphene and simulation [18,27,29,30]. The variation of line width of G band also decrease in case of 4 and 5 layer graphene compared to 1 layer. This is due to the weak interaction of graphene with the substrate and the difference of interlayer force which affect the intra C–C bond vibrations [29,30]. The effect from surface and strain is treated more in Section 6.

5. Electrical properties of multi-layer graphene on GaAs

The electrical characterization required a photolithography process in order to make mesa structures containing Transmission Line Method (TLM) metallic patterns necessary to measure both sheet resistance (R_{sh}) and contact resistance (R_c) independently. The mesa structure was formed using O_2 based RIE for 3 min to remove unnecessary graphene layers followed by GaAs chemical etching with H_3PO_4: H_2O: H_2O_2 (3:50:1) for 2 min. Deposition of metallic electrodes (20 nm Pd and 100 nm Au) were obtained by thermal evaporation and lift-off. A schematic diagram is shown in Fig. 3(d). To form a good Ohmic contact after the metal deposition, the samples were annealed at 450 °C for 5 min under nitrogen atmosphere in a furnace. R_{sh} and R_c were measured before and after annealing.

Multilayer graphene has shown high mobility and low sheet resistance, particularly in its multilayer form, grown on SiC [7,8,31]. When graphene layers are grown on SiC, the layers randomly set and twist, generating a turbostratic structure. The enhancement of turbostratic and incomplete stacking orders indicates that electronic decoupling increase and the electrical properties consequently change [24,25,31]. Few layer CVD graphene also showed better sheet resistance compared to exfoliated graphene [32].

To estimate stacking effects on the electrical properties, the sheet resistance of different samples with increasing number of layers of graphene on GaAs were compared in Fig. 5. On each sample, the sheet resistance was measured at different points and at least 4 devices in order to investigate its uniformity. Contact resistance of 2 and 5 layer graphene before thermal annealing are 15.73 and 6.86 Ω mm, respectively which are changed to 0.07 and 0.05 Ω mm, after thermal annealing (Ohmic annealing). In case of 10 layer graphene, the sheet resistance before thermal annealing is 0.25 Ω mm Fig. 5 shows the average values and error bars of the sheet resistance. The two-layer graphene shows relatively large sheet resistance variations compared with the 4, 5 and 10 layers (see black solid squares and line in Fig. 5). Overall, the sheet resistance tends to decrease with increasing number of stacked layers. CVD graphene showed relatively deteriorated carrier mobility compared to theoretical values due to serious scattering of carriers with defects, surface phonon and impurities [18]. The two-

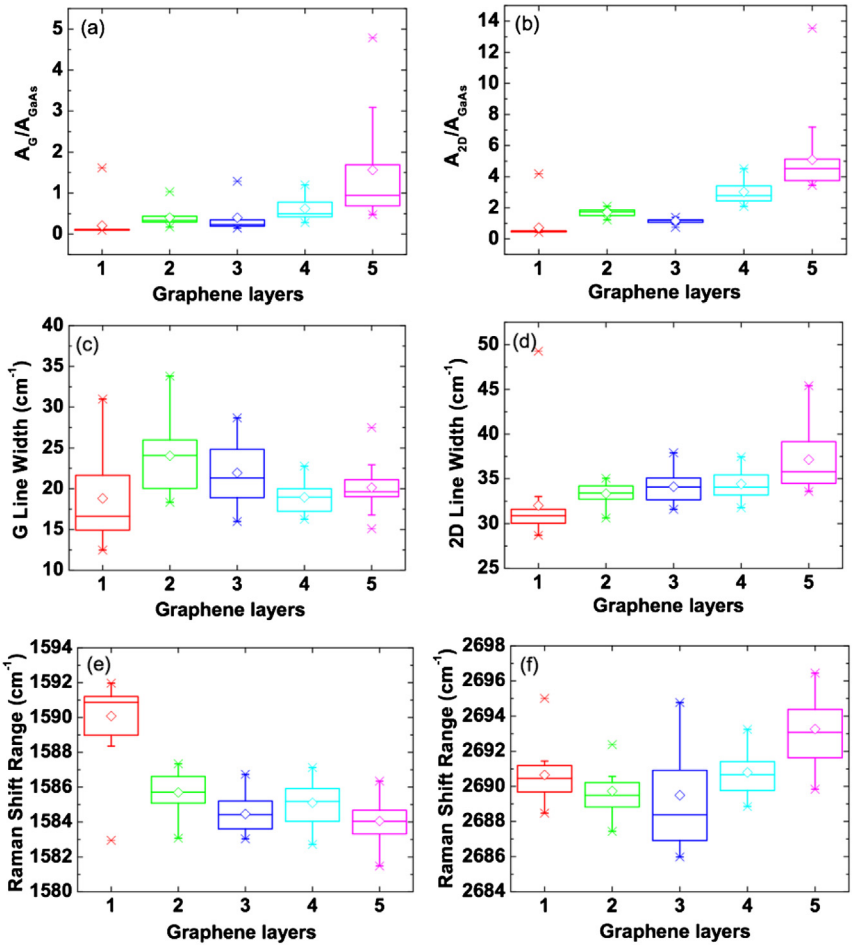

Fig. 4. Variations of results of micro-Raman measurements on different number of graphene layers: (a) Area ratio of G mode of graphene and LO mode of GaAs (290 cm^{-1}), (b) Area ratio of 2D mode of graphene and LO mode of GaAs, (c), (d) change in line width of G and 2D, (e) and (f) Raman shift of G and 2D positions. (A colour version of this figure can be viewed online.)

layer graphene also have tears, particles, and wrinkles (see Fig. 1), which all represent sources of scattering and compromise the sheet resistance as well as the contact resistance. Since, R_{sh} is the ratio of resistivity, ρ, and thickness, t, of the conducting film ($R_{sh} = \rho/t$), where the resistivity (ρ) is related to the carrier mobility and the carrier density, the large number of scattering sources in the two-layer graphene is the cause of the resulting high sheet resistance and large variations. However, enhancement of turborstratic and incomplete stacking in multilayer graphene means that interlayer interaction can be reduced and consequently carrier mobility can be improved. Moreover, not only thicker carrier channel but also increasing unintentional doping improves the sheet resistance, both of which are achieved by increasing the number of layers.

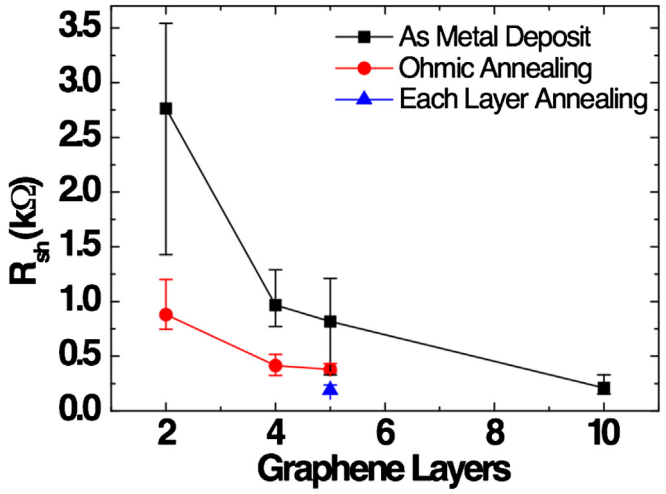

Fig. 5. Variation of sheet resistance with different number of graphene layers before (black solid squares and line) and after 450 °C thermal annealing (red solid circles and line). Absence of the sheet resistance for 10 layers after thermal annealing is due to easy peeling off of the electrode. (A colour version of this figure can be viewed online.)

In Fig. 5, the slope is non-linear with increasing number of layers. This indicates that the mobility and carrier density, rather than thickness of graphene, are the dominant factors in reducing R_{sh}. If impurities such as residual PMMA contamination of the graphene surface are reduced and doping increased, R_{sh} would be further improved. The results of Ohmic annealing at 450 °C after electrode metal deposition show dramatically reduced R_{sh} and its variation (see red solid circles and line in Fig. 5). Over 400 °C annealing temperature, the backbone of residual PMMA can be broken and removed [33]. After annealing, the active sites on graphene easily adsorb H_2O and O_2 molecules that act as p-type dopants in the air [33,34]. Therefore, effectively removed residual PMMA and enhanced carrier density by thermal annealing reduces resistance. The R_{sh} of the 10 layers could not be measured after Ohmic annealing because the metal electrode on graphene easily peeled off, which indicated that the annealing affected adhesion

between each graphene, metals and substrate. The calculated sheet resistance of annealed 10 layer graphene from the existing data of Fig. 5 is 177.4 Ω/□ which is similar to that of pristine 10 layer graphene.

To improve the local electrical uniformity by removing residual polymer and increasing carrier density, thermal annealing was performed after each layer transfer. This was done on a five-layer graphene sample and the result is shown in Fig. 5 (see blue solid triangle). A decrease of the R_{sh}, along with a substantial reduction of its variation (see error bar over the blue solid triangle), is observed. From the same sample we obtained the lowest R_{sh}, corresponding to 164 Ω/□, and the lowest variation of 25% compared to the 59% variation of As Metal Deposition (black solid square at 5-layers). It can be concluded that the uniformity is exceedingly improved after annealing. As mentioned previously, annealing reduces the scattering sources and enhance carrier densities, so that mobilities and amount of charged carriers are more uniform over larger areas in each layer. These are the primary cause of the observed electrical variations. Such R_{sh} and variation were obtained without intentional doping in each layer. Therefore, if each layer is additionally doped with much more effective dopants compared to O_2 or H_2O molecules, the electrical properties and their variations will be improved further.

Therefore a different trend is seen, in sharp contrast to the huge variation observed in the Raman data, with the variation of sheet resistance for different multilayer graphene. The sheet resistance (see Fig. 5) gradually decreases with the increase of the number of layer, which means that utilizing multilayer CVD graphene for electrical device is a useful method to obtain good uniformity of the electrical properties.

6. Induced strain by metal deposition

Any fabrication process carried out over graphene, after its transfer on substrate, affects graphene itself: defects and contaminations reduce the mobility, doping increases the carrier concentration, strain changes graphene's band structure, etc.

It has been shown as strain can be used to functionalize graphene [35–37] and different approaches have been used to attempt to stress a graphene sheet [37–39]. Nevertheless, inducing strain in graphene, in order to change its band structure, remains a major challenge. In an earlier work [40] we showed how surface contamination strains graphene which, consequently, relaxes and generates ripples to release the stress. Metal deposition can, therefore, be another simple way of inducing strain in graphene [41,42].

In the previous section we discussed the fabrication of TLM contacts used to investigate the electrical properties of graphene. Here the same TLM contacts used for the electrical measurements are the surface structures that induce strain on graphene. The Pd/Au TLM electrodes are positioned at a relative distance of each other: 1, 3, 5, and 10 μm separation, as shown in Fig. 3(d).

Raman spectroscopy was used again to prove how external stress affect graphene after metal deposition. The position and linewidth of the G band are deeply related to the strain and doping [43–45]. Especially, local strain can be a dominant factor for the large variation of the G band position. We focus on 1 and 4 layer graphene on GaAs and SiO_2 substrate before and after metal electrode fabrication. The TLM structure is represented in Fig. 6(a), for each pair of contacts we measure four Raman spectrums at equally spaced positions as indicated by the dots in the same figure. Between the contacts graphene is exposed and supported by the substrate: there is no metal absorption in such regions since a lift-off technique was used to pattern the contacts.

Fig. 6(b) shows the G band positions of 1 layer (violet squares) and 4 layer (red circles) graphene on GaAs after the metal electrode deposition. Raman measurements were performed on graphene between two electrodes with different distance, as represented by the dots in Fig. 6(a). The straight lines and gray boxes in Fig. 6 (b) indicate the average value of the G band positions and error ranges obtained from the 16 point Raman maps (see section 2) prior to the metal deposition. In case of the 1 layer on GaAs, graphene between contacts shows a shift towards low frequencies (red shift) of the G band position compared to the value before contacts. This indicate that the contacts introduce tensile strain in the graphene in-between. On the other hand, the 4 layer graphene shows a slightly shift toward higher frequency (blue shift) of the G band after metal deposition compared to the average value of pristine 4 layer before contacts. This suggests that compressive strain is instead induced on graphene between contacts.

Raman spectrums of graphene on GaAs show an intrinsic noise due to the interference of the Raman signal with the luminescence generated by GaAs. This interference is much more severe after metal deposition and this makes very difficult the acquisition of the Raman spectra in case of the 1 and 3 μm separation gap.

Similar measurements, shown in Fig. 6(c), were then performed for the 1 and 4 layer graphene on SiO_2/Si substrate. The 1 layer graphene (green triangles) shows a red shit of the G band position compared to the average value before contacts. The behavior is similar to the 1 layer on GaAs, even though the frequency level shifts are not as large as for GaAs (see Fig. 6(b)). The 4 layer graphene (blue triangle in Fig. 6(c)) on SiO_2 doesn't show a particular shift if compared to the average value without contacts (straight blue line). We consider one of the reason of different trend of G band shift on both substrate is different thermal expansion coefficient of graphene and both substrates. GaAs is a crystal and SiO_2 is amorphous so that during metal evaporation and cooling, graphene is affected from the differently contracted substrates. Chen et al. already reported that there is a G band shift of graphene on Si substrate and suspended with different temperature [44]. They explained G band position of monolayer graphene on the substrate changed as much as 25 cm^{-1} after thermal cycling from 300 K to 700 K while G band of suspended graphene was not much shifted, because graphene was affected from the Si substrate with different thermal expansion coefficient. If we accept this explanation, since GaAs has ten times larger thermal expansion coefficient than SiO_2, the shift of G position is larger than when metal is deposited on graphene.

Although data in Fig. 6 shows some differences for graphene on GaAs or SiO_2/Si substrates, some important factors can be deduced. First, the tensile strain induced by the metal contacts on the 1 layer graphene is evident and is confirmed by a red shift of the G band position for both GaAs and SiO_2. Second, the 4 layer graphene shows a slightly compressive strain (blue shift) for GaAs, which is not observed for the 4 layer on SiO_2. This is might due to a weaker substrate effect which is screened by the 4 stacked graphene layer. The last observation is that the closer to the electrode the wider variation of G position is detected in 4 layer graphene. This indicates that the strain generated by the electrode is different in regions far from the electrode itself, where graphene seems to be more relaxed. Deposited metal electrodes press onto the graphene layer and this pressure can be a source of strain in the graphene area between two electrodes.

7. Conclusion

The repeated manual transfer procedures to obtain multilayer graphene result in random stacking that is a cause of the large variations observed in the optical and electrical properties. Electronic decoupling by turbostratic and incomplete stacking order

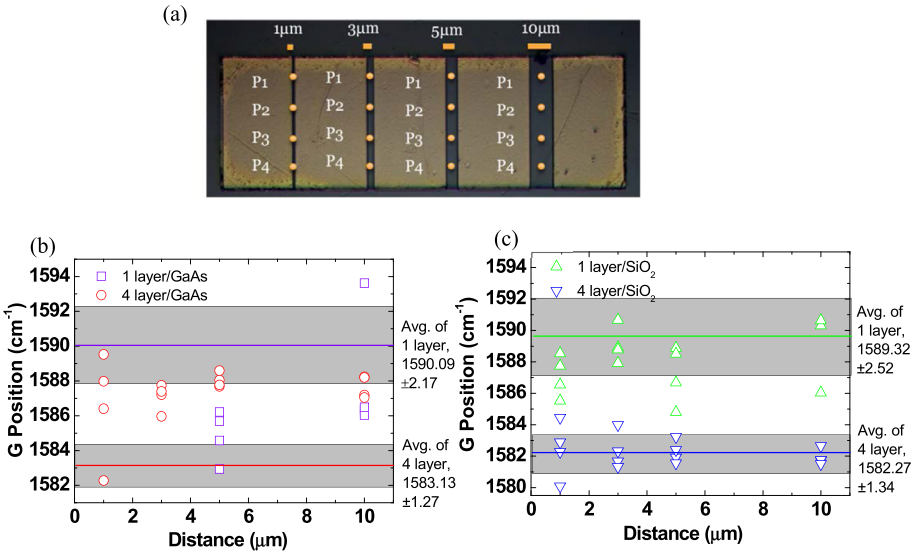

Fig. 6. (a) Raman measurement location of TLM pattern on GaAs, (b) G band shift of 1&4 layer graphene on GaAs before (straight line) and after metal deposition (data points) and (c) G band shift of 1&4 layer graphene on SiO_2 before (straight line) and after metal deposition (data points). (A colour version of this figure can be viewed online.)

make multilayer graphene behave like single layer and increase carrier mobility. Reduced scattering sources like defects and impurities and increasing carrier density of multilayer graphene by each layer thermal annealing improve sheet resistance and electrical uniformity. After metal deposition, graphene showed a change in the Raman response, which indicated the presence of stress. The induced strain (strain is a way for opening a band gap in graphene) was more pronounced for the monolayer on GaAs than the multilayer. Therefore, multilayer graphene have various benefit in that one can control uniformity and substrate effect and alternating regions of multi and monolayer on the semi-insulating GaAs may be the basis for new optoelectronic applications.

Acknowledgment

We are grateful to the Faculty of Engineering and Physical Sciences at the University of Manchester for funding this work and The Ministry of Higher Education and Scientific Research (MOHESR), Iraq.

Appendix A. Supplementary data

Supplementary data related to this article can be found at http://dx.doi.org/10.1016/j.carbon.2015.09.014.

References

[1] K.S. Novoselov, D. Jiang, F. Schedin, T.J. Booth, V.V. Khotkevich, S.V. Morozov, et al., Two-dimensional atomic crystals, Proc. Natl. Acad. Sci. U. S. A. 102 (30) (2005) 10451–10453.
[2] K.S. Novoselov, A.K. Geim, S.V. Morozov, D. Jiang, Y. Zhang, S.V. Dubonos, et al., Electric field effect in atomically thin carbon films, Science 306 (5696) (2004) 666–669.
[3] A.K. Geim, K.S. Novoselov, The rise of graphene, Nat. Mater. 6 (3) (2007) 183–191.
[4] S. De, J.N. Coleman, Are there fundamental limitations on the sheet resistance and transmittance of thin graphene films? ACS Nano 4 (5) (2010) 2713–2720.
[5] Z. Liu, J. Li, Z.-H. Sun, G. Tai, S.-P. Lau, F. Yan, The application of highly doped single-layer graphene as the top electrodes of semitransparent organic solar cells, ACS Nano 6 (1) (2012) 810–818.
[6] C. Riedl, U. Starke, J. Bernhardt, M. Franke, K. Heinz, Structural properties of the graphene-SiC(0001) interface as a key for the preparation of homogeneous large-terrace graphene surfaces, Phys. Rev. B 76 (24) (2007) 245406.
[7] W. Norimatsu, M. Kusunoki, Epitaxial graphene on SiC{0001}: advances and perspectives, Phys. Chem. Chem. Phys. 16 (8) (2014) 3501–3511.
[8] E. Pallecchi, F. Lafont, V. Cavaliere, F. Schopfer, D. Mailly, W. Poirier, et al., High electron mobility in epitaxial graphene on 4H-SiC(0001) via post-growth annealing under hydrogen, Sci. Rep. 4 (2014).
[9] J.D. Wood, S.W. Schmucker, A.S. Lyons, E. Pop, J.W. Lyding, Effects of polycrystalline Cu substrate on graphene growth by chemical vapor deposition, Nano Lett. 11 (11) (2011) 4547–4554.
[10] L. Zhao, K.T. Rim, H. Zhou, R. He, T.F. Heinz, A. Pinczuk, et al., Influence of copper crystal surface on the CVD growth of large area monolayer graphene, Solid State Commun. 151 (7) (2011) 509–513.
[11] S. Bae, H. Kim, Y. Lee, X. Xu, J.-S. Park, Y. Zheng, et al., Roll-to-roll production of 30-inch graphene films for transparent electrodes, Nat. Nano 5 (8) (2010) 574–578.
[12] G. Wang, Y. Kim, M. Choe, T.-W. Kim, T. Lee, A new approach for molecular electronic junctions with a multilayer graphene electrode, Adv. Mater. 23 (6) (2011) 755–760.
[13] Y. Sui, J. Appenzeller, Screening and interlayer coupling in multilayer graphene field-effect transistors, Nano Lett. 9 (8) (2009) 2973–2977.
[14] U.J. Kim, J. Hur, S. Cheon, D.-Y. Chung, H. Son, Y. Park, et al., Enhancement of integrity of graphene transferred by interface energy modulation, Carbon 65 (2013) 165–174.
[15] Y. Zhang, L. Zhang, C. Zhou, Review of chemical vapor deposition of graphene and related applications, Accounts Chem. Res. 46 (10) (2013) 2329–2339.
[16] X. Li, Y. Zhu, W. Cai, M. Borysiak, B. Han, D. Chen, et al., Transfer of large-area graphene films for high-performance transparent conductive electrodes, Nano Lett. 9 (12) (2009) 4359–4363.
[17] K. Yan, H. Peng, Y. Zhou, H. Li, Z. Liu, Formation of bilayer bernal graphene: layer-by-layer epitaxy via chemical vapor deposition, Nano Lett. 11 (3) (2011) 1106–1110.
[18] H. Jih-Shang, L. Yu-Hsiang, H. Jeong-Yuan, C. Railing, C. Surojit, C. Chang-Jiang, et al., Imaging layer number and stacking order through formulating Raman fingerprints obtained from hexagonal single crystals of few layer graphene, Nanotechnology 24 (1) (2013) 015702.
[19] A.C. Ferrari, D.M. Basko, Raman spectroscopy as a versatile tool for studying the properties of graphene, Nat. Nano 8 (4) (2013) 235–246.
[20] J. Liu, Q. Li, Y. Zou, Q. Qian, Y. Jin, G. Li, et al., The dependence of graphene Raman D-band on carrier density, Nano Lett. 13 (12) (2013) 6170–6175.
[21] M. Bruna, A.K. Ott, M. Ijäs, D. Yoon, U. Sassi, A.C. Ferrari, Doping Dependence of the Raman Spectrum of Defected Graphene, ACS Nano 8 (7) (2014) 7432–7441.
[22] A.C. Ferrari, J.C. Meyer, V. Scardaci, C. Casiraghi, M. Lazzeri, F. Mauri, et al., Raman spectrum of graphene and graphene layers, Phys. Rev. Lett. 97 (18) (2006) 187401.
[23] X. Li, W. Cai, J. An, S. Kim, J. Nah, D. Yang, et al., Large-Area Synthesis of High-Quality and Uniform Graphene Films on Copper Foils, Science 324 (5932) (2009) 1312–1314.
[24] C. Faugeras, A. Nerrière, M. Potemski, A. Mahmood, E. Dujardin, C. Berger, et al., Few-layer graphene on SiC, pyrolitic graphite, and graphene: a Raman scattering study, Appl. Phys. Lett. 92 (1) (2008) 011914.
[25] J. Hass, F. Varchon, J.E. Millán-Otoya, M. Sprinkle, N. Sharma, W.A. de Heer, et al., Why multilayer graphene on 4H-SiC(000-1) behaves like a single sheet of graphene, Phys. Rev. Lett. 100 (12) (2008) 125504.
[26] J.S. Park, A. Reina, R. Saito, J. Kong, G. Dresselhaus, M.S. Dresselhaus, G' band Raman spectra of single, double and triple layer graphene, Carbon 47 (5)

(2009) 1303–1310.
[27] D. Graf, F. Molitor, K. Ensslin, C. Stampfer, A. Jungen, C. Hierold, et al., Spatially resolved Raman spectroscopy of single- and few-layer graphene, Nano Lett. 7 (2) (2007) 238–242.
[28] D.R. Lenski, M.S. Fuhrer, Raman and optical characterization of multilayer turbostratic graphene grown via chemical vapor deposition, J. Appl. Phys. 110 (1) (2011) 013720.
[29] A. Gupta, G. Chen, P. Joshi, S. Tadigadapa, Raman Scattering from high-frequency phonons in supported n-graphene layer films, Nano Lett. 6 (12) (2006) 2667–2673.
[30] J.-W. Jiang, H. Tang, B.-S. Wang, Z.-B. Su, Raman and infrared properties and layer dependence of the phonon dispersions in multilayered graphene, Phys. Rev. B 77 (23) (2008) 235421.
[31] Y.R. Hernandez, S. Schweitzer, J.-S. Kim, A.K. Patra, J. Englert, I. Lieberwirth, et al., Turbostratic Graphitic Microstructures: Electronically Decoupled Multilayer Graphene Devices with Robust High Charge Carrier Mobility, 2013 arXiv:13016087. Jan 2013 ed. arXiv:1301.6087: arXiv:1301.6087.
[32] T.H. Yu, C.W. Liang, C. Kim, E.S. Song, B. Yu, Three-dimensional stacked multilayer graphene interconnects, Ieee Electron Device Lett. 32 (8) (2011) 1110–1112.
[33] Y. Ahn, H. Kim, Y.-H. Kim, Y. Yi, S.-I. Kim, Procedure of removing polymer residues and its influences on electronic and structural characteristics of graphene, Appl. Phys. Lett. 102 (9) (2013) 091602.
[34] Z.H. Ni, H.M. Wang, Z.Q. Luo, Y.Y. Wang, T. Yu, Y.H. Wu, et al., The effect of vacuum annealing on graphene, J. Raman Spectrosc. 41 (5) (2010) 479–483.
[35] V.M. Pereira, A.H. Castro Neto, N.M.R. Peres, Tight-binding approach to uniaxial strain in graphene, Phys. Rev. B 80 (4) (2009) 045401.
[36] R.M. Ribeiro, M.P. Vitor, N.M.R. Peres, P.R. Briddon, A.H.C. Neto, Strained graphene: tight-binding and density functional calculations, New J. Phys. 11 (11) (2009) 115002.
[37] F. Guinea, M.I. Katsnelson, A.K. Geim, Energy gaps and a zero-field quantum Hall effect in graphene by strain engineering, Nat. Phys. 6 (1) (2010) 30–33.
[38] T.M.G. Mohiuddin, A. Lombardo, R.R. Nair, A. Bonetti, G. Savini, R. Jalil, et al., Uniaxial strain in graphene by Raman spectroscopy: G peak splitting, Grüneisen parameters, and sample orientation, Phys. Rev. B 79 (20) (2009) 205433.
[39] S.M. Clark, K.-J. Jeon, J.-Y. Chen, C.-S. Yoo, Few-layer graphene under high pressure: Raman and X-ray diffraction studies, Solid State Commun. 154 (2013) 15–18.
[40] U. Monteverde, J. Pal, M.A. Migliorato, M. Missous, U. Bangert, R. Zan, et al., Under pressure: control of strain, phonons and bandgap opening in rippled graphene, Carbon 91 (2015) 266–274.
[41] W.X. Wang, S.H. Liang, T. Yu, D.H. Li, Y.B. Li, X.F. Han, The study of interaction between graphene and metals by Raman spectroscopy, J. Appl. Phys. 109 (7) (2011) 07C501.
[42] H. Shioya, M.F. Craciun, S. Russo, M. Yamamoto, S. Tarucha, Straining graphene using thin film shrinkage methods, Nano Lett. 14 (2014) 1158–1163.
[43] I. Calizo, W. Bao, F. Miao, C.N. Lau, A.A. Balandin, The effect of substrates on the Raman spectrum of graphene: graphene-on-sapphire and graphene-on-glass, Appl. Phys. Lett. 91 (20) (2007) 201904.
[44] C.-C. Chen, W. Bao, J. Theiss, C. Dames, C.N. Lau, S.B. Cronin, Raman spectroscopy of ripple formation in suspended graphene, Nano Lett. 9 (12) (2009) 4172–4176.
[45] R. Yang, Q.S. Huang, X.L. Chen, G.Y. Zhang, H.-J. Gao, Substrate doping effects on Raman spectrum of epitaxial graphene on SiC, J. Appl. Phys. 107 (3) (2010) 034305.